Harmonic analysis of thyristor controlled series capacitor in polluted Algerian network

Mohamed Nassim Kraimia* and
Mohamed Boudour

Department of Electrical Engineering,
Laboratory of Electrical and Industrial Systems,
University of Science and Technology Houari Boumediene,
El Alia 16111, Bab Ezzouar, Algiers, Algeria
Email: kraimia.nassim@yahoo.fr
Email: mboudour@ieee.org
*Corresponding author

Abstract: This paper presents the study of the impact of harmonic distortion generated by the thyristors controlled series capacitor (TCSC) in Algerian electric power system. By applying Fourier transform of terminal voltage and switching function, the TCSC model is used as a harmonic admittance matrix, in the frequency domain, and then integrated into a balanced harmonic load flow algorithm based on the Newton-Raphson method. The study has been carried out with the equivalent Algerian power system 114 bus. The total harmonics and RMS voltages are evaluated under different operating regions of the TCSC.

Keywords: harmonic power flow; nonlinear load; thyristors controlled series capacitor; TCSC; Algerian power system; total harmonic distortion.

Reference to this paper should be made as follows: Kraimia, M.N. and Boudour, M. (2021) 'Harmonic analysis of thyristor controlled series capacitor in polluted Algerian network', *Int. J. Energy Technology and Policy*, Vol. 17, No. 1, pp.86–97.

Biographical notes: Mohamed Nassim Kraimia received his Magister degree in Power System Network from the Faculty of Electrical Engineering and Electronic; University of Hadj Lakhdar Batna- of Algiers in 2007. Currently, he is a PHD student at the Faculty of Electrical Engineering and Computing; University of Sciences and Technology Houari Boumediene (USTHB) of Algiers and works as an Electrical Engineer at the Electrical Algerian Company (Sonelgaz/Distribution Power System) since 2009. His current research interest includes power system (transmission and distribution) computing and simulation and control, FACTS devices, power quality, renewable energy.

Mohamed Boudour received the BSc, MSc and PhD in Electrical Engineering from the Polytechnic School of Algiers in 1991, 1994 and 2004, respectively. Since January 1994, he has been with the University of Sciences and Technology Houari Boumediene of Algiers (USTHB) as a Teacher and Researcher. He was awarded as a Fulbright fellowship at the University of Washington, Seattle (USA) from 2005–2006. He is a member of the executive committee of ARELEC (Algerian CIGRE) and IEEE senior member since 2007. His main interests are power systems stability and control using intelligent programming, integration of renewable energy sources in smart grids. Currently, he is the Director of Electrical and Industrial System Laboratory.

1 Introduction

With the increase of electronic devices use in power systems, the problem related to harmonic distortion becomes a very important issue. These harmonics have a significant impact on power systems such as: communication interference, protection system malfunctioning, transmission lines overheating, reduction of the equipment life and more. Furthermore, the analysis of harmonics in power systems, including nonlinear loads is crucial (Romero et al., 2011).

In particular, harmonic load flow is used for harmonic analysis problem to give information related to nodal voltage and branch current at each frequency of interest. However, based on this information, an operator may either predict a resonance problem that could be appeared at each harmonic, or evaluate the total harmonic distortion of voltage and current waveforms. In the literature, several approaches have been performed to solve the harmonic power flow problem. In Xia and Heydt (1982a, 1982b), the conventional power flow was reformulated to include the nonlinear loads. In Lin et al. (2004) and Moreno and Usaola (2004), the previous method was extended to include unbalance system. In Smith and Arrillaga (1999), a model of the converter was established and included in the algorithm. Norton equivalent model of nonlinear load was well presented in Thunberg and Soder (1999). In this paper, the harmonic analysis is based on the algorithm developed by Xia and Heydt (1982a), because it considers the harmonic interaction between the AC transmission system and the nonlinear loads. The problem solution is then obtained using the Newton-Raphson method. The increase of the power demand could provide some constrained operating conditions such as system saturation, and therefore voltage drops may also exist in all power system nodes. The TCSC as a flexible AC transmission system (FACTS) technology has two regions, namely inductive and capacitive regions governed by a system of anti-parallel thyristors that allows the control of reactive current derived by the thyristor controlled reactor (TCR) branch. It is mainly used for increasing power transfer capability and improving system transient stability. Recently, considerable effort has been dedicated to investigate the series compensation effects in power systems in fundamental frequency (Fuerte-Esquivel et al., 2000). The discontinuous reactive current derived by TCR branch remains flowing in TCSC loop circuit and results in a distortion of TCSC capacitor voltage. Therefore, deriving a harmonic model of TCSC in the frequency domain is essential to determine their interaction with the AC system.

Many works in the literature have treated the TCSC harmonic modelling. In Kai et al. (1999) the TCSC device was modelled as voltage and current sources. The obtaining results show that these models are not able to give accurate information about the interaction between the nonlinear load and the other AC system components. Another model that represents the TCSC as harmonic impedance source was used to investigate the interaction between the TCSC and a simplified radial transmission system with linear and nonlinear loads (Chavez and Ramirez, 2006; García et al., 2014). These studies were handled only in capacitive region. In today power systems containing a variety of nonlinearities, the impact of TCSC on the compensated transmission line is very important.

In this paper, the TCSC is represented as a harmonic admittance matrix used at each frequency. The proposed algorithm has been tested for Algerian electric power system

114 buses in the presence of eight odd order harmonics: 5th; 7th; 11th; 13th; 17th; 19th; 23th; 25th.

2 Modelling of TCSC in the harmonic domain

The TCSC is one of the most system FACTS, used to expand the transmission facilities and the stability enhancement. It contains an anti-parallel reactance branch called thyristor controlled reactor (TCR), with series capacitor as shown in Figure 1. The thyristors Th_1 and Th_2 are gated on twice in each cycle, controlling the reactive current derived by the TCR. This current can be found by integrating the voltage across the reactor V_R multiplied by a switching function $H(t)$ (Sen and Sen, 2009). The latter is schematically shown in Figure 2 has two states: 1 – when the thyristor is ON and 0 – when the thyristor turns OFF.

Figure 1 One module of TCSC circuit (see online version for colours)

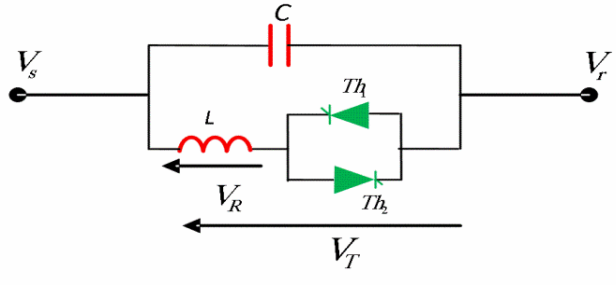

Figure 2 Switching function H(t) (see online version for colours)

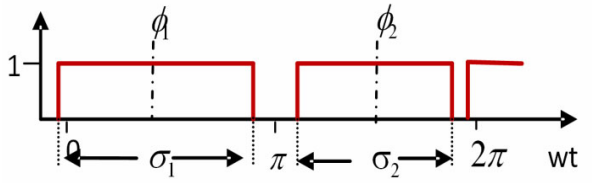

Assuming that the voltage across the TCR and switching function H are periodic. By applying a complex Fourier series of two waveforms, we obtain the following expressions:

$$V_T = \sum_{m=-\infty}^{+\infty} V_{Tm} e^{j(mwt)} \tag{1}$$

$$H = \sum_{n=-\infty}^{+\infty} h_n \left(\sigma_1, \phi_1, \sigma_2, \phi_2\right) e^{j(nwt)} \tag{2}$$

where V_{Tm} is the m^{th} harmonic coefficient of the terminal voltage V_T, and h_n is n^{th} harmonic coefficient of the switching function H. From Figure 2, σ is the conduction

angle and ϕ is the centre of the conduction period. The harmonic magnitude of switching function is given by:

$$h_n = \frac{1}{2\pi} \int_{t1}^{t1+2\pi} H(t) e^{-j(nwt)} dwt \tag{3}$$

In the harmonic domain, the voltage across the inductor V_R is given by:

$$V_R(t) = V_T H = \sum_{m,n=-\infty}^{\infty} V_{Tm} h_n e^{j(m+n)wt} \tag{4}$$

Equation (4) can be expressed as a matrix form, consisting of an infinite magnitude of switching function multiplied by a terminal voltage vector of the TCR.

$$\begin{bmatrix} \vdots \\ V_{R-3} \\ V_{R-2} \\ V_{R-1} \\ \vdots \end{bmatrix} = \begin{bmatrix} . & \vdots & \vdots & \vdots & . \\ \cdots & h_0 & h_{-1} & h_{-2} & \cdots \\ \cdots & h_1 & h_0 & h_{-1} & \cdots \\ \cdots & h_2 & h_1 & h_0 & \cdots \\ . & \vdots & \vdots & \vdots & . \end{bmatrix} \begin{bmatrix} \vdots \\ V_{T-3} \\ V_{T-2} \\ V_{T-1} \\ \vdots \end{bmatrix} \tag{5}$$

where matrix H has a Toeplitz form. It represents a cross coupling between harmonics which is an important characteristic in switching function. By referring to the models used in Bohmann and Lasseter (1989), the harmonic admittance matrix for the TCR and capacitor are given respectively as follows:

$$Y_{TCR} = [LD(Jhw)]^{-1} H \tag{6}$$

$$Y_C = C[D(Jhw)] \tag{7}$$

where D is the differentiation matrix and L is the reactor inductance, and C is the capacitance of series capacitor. The TCSC is well described by two parallel branches of the TCR in (6) and capacitor admittance in (7) and it can be written as:

$$Y_{TCSC} = Y_C + Y_{TCR} \tag{8}$$

This model represents the harmonic admittance matrix of TCSC in steady state, where all the harmonics and cross-coupling between them are clearly represented (Martinez, 2001). Unlike the TCR, the calculation of the harmonic coefficients of the switching matrix corresponding to Y_{TCSC} is found with the terminal voltage difference.

3 Integrating harmonic admittance matrix of TCSC in HPF

TCSC modelling is used to represent the device under a given condition in the frequency domain. This model is integrated into the harmonic load flow program in order to study their effect on the network. The most used three methods in literature are:

1 equivalent power injection (Garcia et al., 2000)

2 creation of a fictitious node (Gotham and Heydt, 1998)

3 modification of the admittance matrix (Preedavichit and Srivastava, 1998).

The last technique is used in this paper to include the TCSC model in power system. Figure 3 shows a TCSC device installed between line $i - j$.

Figure 3 Transmission system with embedded TCSC

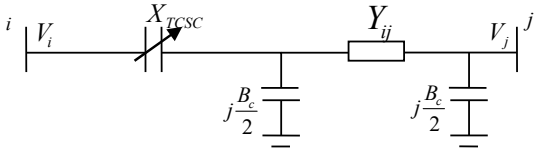

At fundamental frequency, the equivalent admittance of the line between buses i and j is determined and substituted to the line admittance without TCSC and is modified as follows:

$$Y_{ij} = \begin{pmatrix} y'_{ij} + \frac{y_{ij0}}{2} & -y'_{ij} \\ -y'_{ij} & y'_{ij} + \frac{y_{ij0}}{2} \end{pmatrix} \tag{9}$$

where

$$y'_{ij} = \frac{1}{r_{ij} + j\left(fx_{ij} + x_{TCSC}\right)} \tag{10}$$

where y'_{ij}, y_{ij0} are the series and shunt admittance respectively.

The equivalent harmonic admittance of the line between buses i and j is formulated at each harmonic frequency (m) in the system as a same way than the fundamental frequency:

$$Y_{ij}^{m} = \begin{pmatrix} y'^{m}_{ij} + \frac{y^{m}_{ij0}}{2} & -y'^{m}_{ij} \\ -y'^{m}_{ij} & y'^{m}_{ij} + \frac{y^{m}_{ij0}}{2} \end{pmatrix} \tag{11}$$

where y_{ij}^{m} is the m^{th} harmonic admittance of the line between buses my and j with the presence of TCSC.

4 Iterative harmonic analysis algorithm

The first step of the harmonic load flow program consists of modelling the linear components of electrical power system (transmission lines, transformers, generator, and capacitor bank) and nonlinear load as (electronic devices, arc furnace, converters) at fundamental and harmonic frequencies. The Newton's method is used to forcing the appropriate mismatch vector (ΔM) containing of mismatch power (ΔW) and mismatch

current (ΔI) to zero using a Jacobin matrix J and obtaining appropriate correction terms (ΔU).

$$\Delta M = [J]\Delta U^{\xi} \tag{12}$$

$$\Delta U^{\xi} = U^{\xi} - U^{\xi+1} \tag{13}$$

where ξ is the iteration number.

The matrix formulation of the problem is:

$$\begin{bmatrix} \overline{\Delta V}^{(1)} \\ \overline{\Delta V}^{(5)} \\ \overline{\Delta V}^{(7)} \\ \cdot \\ \cdot \\ \cdot \\ \overline{\Delta V}^{(L)} \\ \overline{\Delta\varphi} \end{bmatrix} = \begin{bmatrix} \overline{J}^{(1)} & \overline{J}^{(5)} & \cdots & \overline{J}^{(L)} & 0 \\ \overline{YG}^{(5,1)} & \overline{YG}^{(5,5)} & \cdots & . & \overline{H}^{(5)} \\ \overline{YG}^{(7,1)} & \overline{YG}^{(7,5)} & \cdots & . & \overline{H}^{(7)} \\ . & . & . & . & . \\ . & . & . & . & . \\ . & . & . & . & . \\ \overline{YG}^{(L,1)} & \overline{YG}^{(L,5)} & \cdots & \overline{YG}^{(L,L)} & \overline{H}^{(L)} \\ \overline{YG}^{(1,1)} & \overline{YG}^{(1,5)} & \cdots & \overline{YG}^{(1,L)} & \overline{H}^{(1)} \end{bmatrix}^{-1} \begin{bmatrix} \overline{\Delta W} \\ \overline{\Delta I}^{(5)} \\ \overline{\Delta I}^{(7)} \\ \cdot \\ \cdot \\ \cdot \\ \overline{\Delta I}^{(L)} \\ \overline{\Delta I}^{(1)} \end{bmatrix} \tag{14}$$

Where all elements in this matrix (14), are sub-vectors and sub-matrices partitioned from ΔM, J and ΔU.

The fundamental and total power mismatches are given by:

$$\begin{aligned} \overline{\Delta W} = \Big[& P_2^{(1)} + F_{r,2}^{(1)}, Q_2^{(1)} + F_{i,2}^{(1)}, \ldots, P_{m-1}^{(1)} + F_{r,m-1}^{(1)}, Q_{r,m-1}^{(1)} + F_{i,m-1}^{(1)}, \ldots, \\ & \Delta P_m^{nonlinear}, \Delta Q_m^{nonlinear}, \Delta P_n^{nonlinear}, \Delta Q_n^{nonlinear} \Big] \end{aligned} \tag{15}$$

where

- $P_j^{(1)}, Q_j^{(1)}$ are the fundamental real and reactive load power for the linear bus j
- $F_{r,j}^{(1)}, F_{i,j}^{(1)}$ are the fundamental real and reactive line powers for the linear bus j
- $\Delta P_m^{nonlinear}, \Delta_{mn}^{nonlinear}$ are the totals real and reactive mismatch power for the nonlinear bus m.

The fundamental current mismatch $\Delta I^{(1)}$ is defined only for nonlinear buses, where all currents (e.g., fundamental real and reactive line currents Ir,m(1) , Ii,m(1)and fundamental real and reactive nonlinear load currents Gr,m(1) , Gi,m(1)) are referred to the swing bus and is given by:

$$\overline{\Delta I}^{(1)} = \Big[I_{r,m}^{(1)} + G_{r,m}^{(1)}, I_{i,m}^{(1)} + G_{i,m}^{(1)}, \ldots, I_{r,n}^{(1)} + G_{r,n}^{(1)}, I_{i,n}^{(1)} + G_{i,n}^{(1)} \Big]^t \tag{16}$$

The harmonic current mismatch $\Delta I^{(h)}$ that contains harmonic real and reactive line currents $I_{r,m}^{(h)}$, $I_{i,m}^{(h)}$ and harmonic real and reactive nonlinear load currents $G_{r,m}^{(h)}$, $G_{i,m}^{(h)}$, is defined for linear and nonlinear buses including swing bus as follow:

$$\overline{\Delta I}^{(h)} = \left[I_{r,1}^{(h)}, I_{i,1}^{(h)}, \ldots, I_{r,m-1}^{(h)}, I_{i,m-1}^{(h)}, I_{r,m}^{(h)} + G_{r,m}^{(h)}, I_{i,m}^{(h)} + G_{i,m}^{(h)}, \ldots, I_{r,n}^{(h)} + G_{r,n}^{(h)}, I_{i,n}^{(h)} + G_{i,n}^{(h)} \right]^t \quad (17)$$

The formulation of Jacobin matrix J is well described in Fuchs and Masoum (2008).

5 Case study and simulation results

A computer program performed in MATLAB version 7.0 considering the models and methods described above, has been tested on the equivalent Algerian electric power system 114 buses which has two voltage levels (220/60) KV; the line and bus data of the system are given in Amrane et al. (2017). The test system shown in Figure 4 consists of 175 transmission lines, 15 generators, 99 load buses and 17 tap changer transformers, the total real and reactive power demand are 3,146.2 MW and 1,799.4 MVAR. The system data and results are based on 100 MVA where bus 4 is selected as slack bus. There are five harmonic sources located at load buses 12, 32, 33, 66 and 67 with eight harmonic components for each one as indicated in Tables A1 and A2. Since the TCSC cost is expensive, it is important to choose the best location. Thus, based on the FSVI sensitivity index (Amrane and Boudour, 2014), the line 112 (between buses 41–49) was chosen as the weakest line. The TCSC parameters have been selected with capacitance (X_C = 0.2112 pu) and inductance (X_L = 0.0939 pu) for 50% of compensation level as shown in Table A.3.

Figure 4 Algerian electric power system map (see online version for colours)

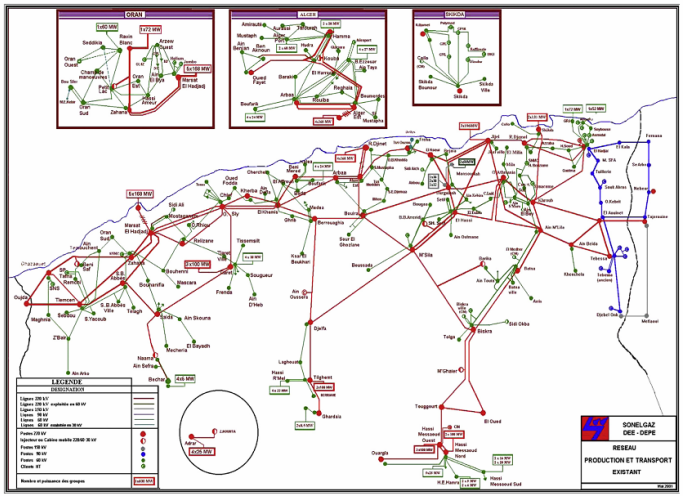

The fundamental and harmonic reactance of TCSC is found from its harmonic impedance matrix by selecting only the diagonal element at a corresponding harmonic frequency of the same harmonic order. Figure 5(a) represents the fundamental reactance variation at line number 112 (between buses 41 and 49) as a function of firing angle (measured from zero crossing capacitor voltage).

Figure 5 TCSC reactance in compensated line (20), (a) fundamental reactance (b) harmonic reactance at each frequency (see online version for colours)

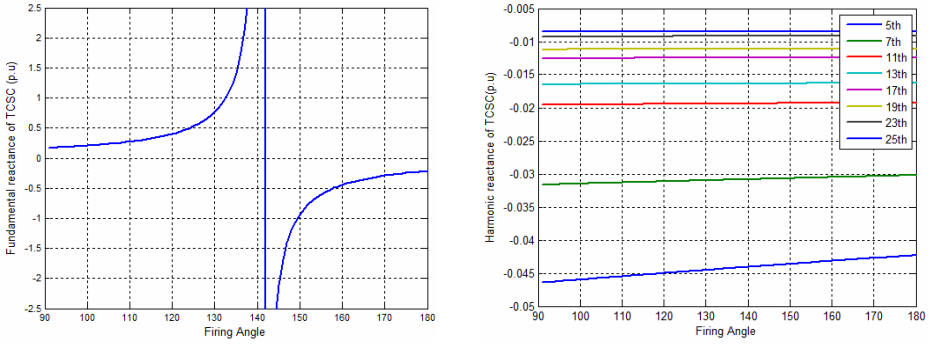

(a) (b)

We notice the presence of three operating regions, namely: inductive region, capacitive region, and resonance region. The last region occurs when the parallel inductive and capacitive reactance have the same values, therefore it must be avoided. From the harmonic admittance matrix at each frequency illustrated in Figure 5(b), it is clear that there is no resonance region and the harmonic reactance at each frequency of interest increases gradually as the firing angle increases. The variation is greater for low order harmonics and smaller for high order harmonics.

Figure 6 RMS Voltage at all buses with and without TCSC (see online version for colours)

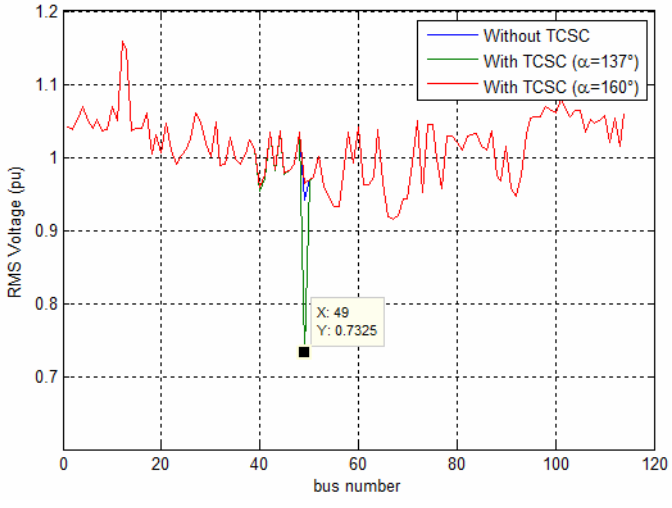

In the inductive region, the fundamental reactance begins from a total equivalent impedance at which the inductive and capacitive reactance XC||XL are in parallel, to infinity value (when the resonance region occurs). Hence, this region operates for firing angle range $90° < \alpha < 140°$. If the firing angle is between $150° < \alpha < 180°$, the reactance is decreasing from infinity value (parallel resonance) to purely capacitive reactance.

Two types of results are often necessary to show the TCSC impact in the harmonic analysis. They are:

a the RMS voltage at all busses

b the THD voltage at all buses.

These results were carried out with TCSC firing angle in inductive (α = 137°) and capacitive region (α = 160°) as well as without the presence of TCSC.

Figure 7 THD Voltage at all buses with and without TCSC (see online version for colours)

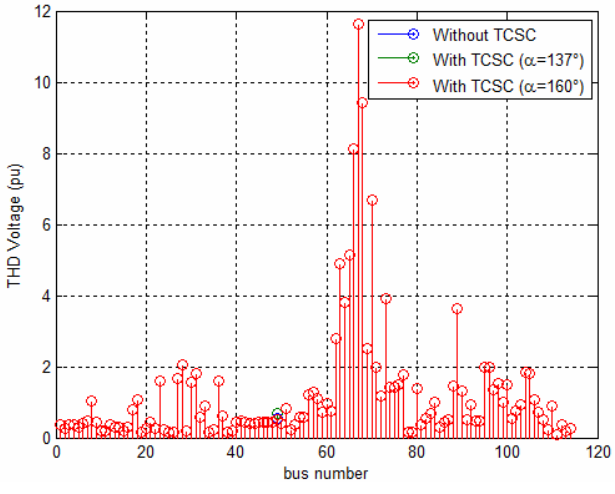

Using the harmonic power flow program with precision of 10^{-6} and by including the obtained fundamental and harmonic reactance, the nodal voltage at all buses and current within all branches can be found. Based on the nodal voltage results, the RMS voltage and THD voltage were calculated at each bus for all firing angle values. Figure 6 shows the RMS voltage at all buses when TCSC operate in inductive and capacitive regions. In these system configurations, the RMS voltage for three cases, matches well at all buses except there is a significant change at load bus 49, where its voltage value drop to 0.7325 due to TCSC control action in inductive region. From Figure 7, the THD voltage is very high at buses 67, 68, 69, because they carry highest harmonic components injected by two neighbours harmonic sources connected by buses 66, 67, while at the other buses the distortion are accepted accordingly to IEEE standards. Since the THD voltage variation is very small with two selected firing angles, in Figures 8(a), 8(b), 8(c) and 8(d). The THD voltage was plotted again for all firing angles. These figures include the THD voltage variation as a function of firing angle at TCSC buses (41 and 49) and harmonic source buses (67–12). It is clearly seen that, there is an exponential behaviour due to TCSC action control, and the variation is greater at the two buses which are close to TCSC location (49, 41) and a little variation at the buses (12, 67) which are far from this device. Thus, the THD voltage variation is little even at high distorted buses. It is also shown that, in some cases, the TCSC could provide an improved effect to the distortion voltage with capacitive control action.

Figure 8 THD voltage variation of buses (49, 41, 67, 12) as function of all firing angles, (a) THD voltage at bus 49 (b)THD voltage at bus 41 (c) THD voltage at bus 67 (d) THD voltage at bus 12 (see online version for colours)

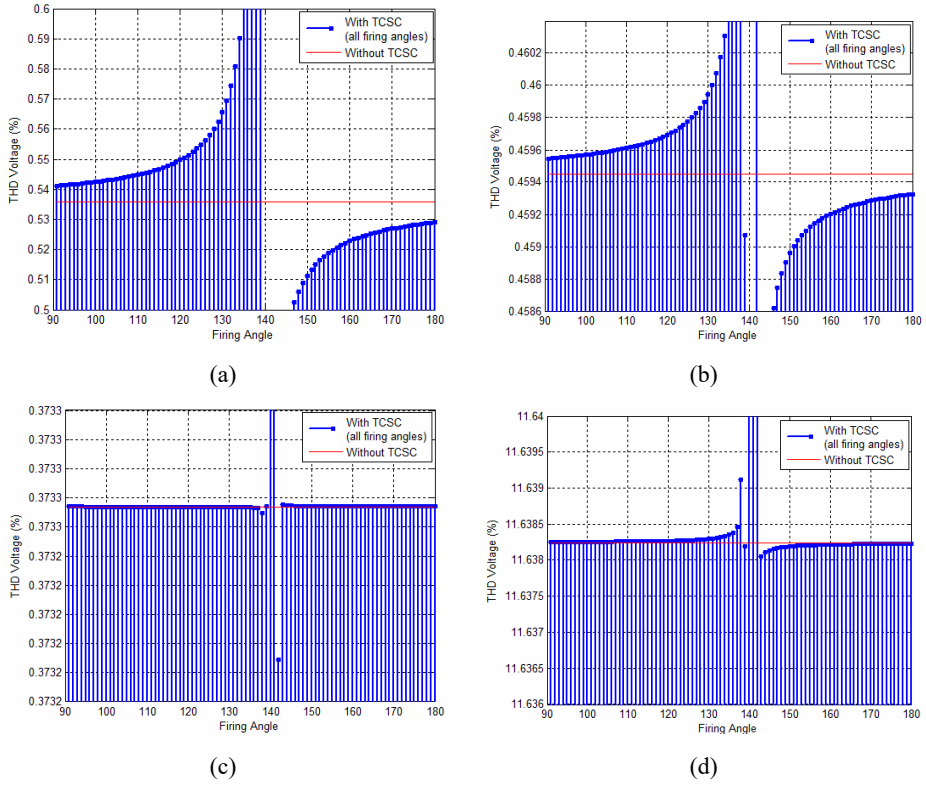

From these obtained results, it can be observed that the TCSC has a significant effect on fundamental magnitude and negligible, one on harmonic components due to the small impact of TCSC harmonic reactance as described in Figure 5(b). However, The TCSC harmonic impedance is very lower with respect to impedance of the AC network, yielding the harmonic components derived by TCR branch remain flowing within the loop circuit (L-C) and do not flow into the AC system.

6 Conclusions

In this paper, a new harmonic analysis formulation was applied in equivalent Algerian network with presence of thyristors controlled series capacitor harmonic impact. The TCSC model was developed using harmonic admittance matrix in order to study the TCSC harmonic impact with different firing angles. By using harmonic power flow, the problems are solved, the nodal voltages at all buses and currents at all branches are found at fundamental and harmonic frequencies. According to the obtained results, the TCSC has a direct impact on RMS voltage as well as THD voltage while a negligible impact was observed in harmonic components due to loop circuit (L-C). Finally, the THD voltage variation was observed well in compensated line and could be improved in

capacitive region, on the other hand its variation is very low, even at the high distorted bus if located so far from TCSC device.

In respect to further work, we aim to find the best location of the TCSC in a larger power system using intelligent techniques under non-sinusoidal conditions.

References

Amrane, Y. and Boudour, M. (2014) 'Particle swarm optimization based reactive power planning for voltage stability improvement', *Electrical Sciences and Technologies in Maghreb (CISTEM)*, pp.1–7.

Amrane, Y., Elmaouhab, A., Boudour, M. and Ladjici, A.A. (2017) 'Voltage stability analysis based on multi-objective optimal reactive power dispatch under various contingency', *International Journal on Electrical Engineering and Informatics*, Vol. 9, No. 3, pp.521–541.

Bohmann, L.J. and Lasseter, R.H. (1989) 'Harmonic interactions in thyristor controlled reactor circuits', *IEEE Transactions on Power Delivery*, Vol. 4, No. 3, pp.1919–1926.

Chavez, J. and Ramirez, A. (2006) 'SVC and TCSC implemented into a Newton-type harmonic power flow algorithm', *38th North American Power Symposium 2006 (NAPS 2006)*, pp.283–287.

Fuchs, E. and Masoum, M.A. (2008) *Power Quality in Power Systems and Electrical Machines*, Elsevier Academic Press, USA [online] https://www.elsevier.com/books/power-quality-in-power-systems-and-electrical-machines/fuchs/978-0-12-369536-9.

Fuerte-Esquivel, C., Acha, E. and Ambriz-Perez, H. (2000) 'A thyristor controlled series compensator model for the power flow solution of practical power networks', *IEEE Transactions on Power Systems*, Vol. 15, No. 1, pp.58–64.

García, H., Segundo, J. and Madrigal, M. (2014) 'Harmonic analysis of power systems including thyristor-controlled series capacitor (TCSC) and its interaction with the transmission line', *Electric Power Systems Research*, Vol. 106, pp.151–159 [online] https://www.sciencedirect.com/journal/electric-power-systems-research/vol/106/suppl/C.

Garcia, P.A., Pereira, J.L.R., Carneiro, S., Da Costa, V.M. and Martins, N. (2000) 'Three-phase power flow calculations using the current injection method', *IEEE Transactions on Power Systems*, Vol. 15, No. 2, pp.508–514.

Gotham, D.J. and Heydt, G. (1998) 'Power flow control and power flow studies for systems with FACTS devices', *IEEE Transactions on Power Systems*, Vol. 13, No. 1, pp.60–65.

Kai, T., Takeuchi, N., Sato, T. and Akagi, H. (1999) 'A study of thyristor controlled series capacitor models for power system stability analysis', *Electrical Engineering in Japan*, Vol. 129, No. 1, pp.20–28.

Lin, W-M., Zhan, T-S. and Tsay, M-T. (2004) 'Multiple-frequency three-phase load flow for harmonic analysis', *IEEE transactions on Power Systems*, Vol. 19, No. 2, pp.897–904.

Martinez, M.M. (2001) *Modelling of Power Electronics Controllers for Harmonic Analysis in Power Systems*, University of Glasgow.

Moreno, M.Á. and Usaola, J. (2004) 'A new balanced harmonic load flow including nonlinear loads modeled with RBF networks', *IEEE Transactions on Power Delivery*, Vol. 19, No. 2, pp.686–693.

Preedavichit, P. and Srivastava, S. (1998) 'Optimal reactive power dispatch considering FACTS devices', *Electric Power Systems Research*, Vol. 46, No. 3, pp.251–257.

Romero, A., Zini, H., Rattá, G. and Dib, R. (2011) 'Harmonic load-flow approach based on the possibility theory', *IET Generation, Transmission & Distribution*, Vol. 5, No. 4, pp.393–404.

Sen, K.K. and Sen, M.L. (2009) *Introduction to FACTS Controllers: Theory, Modeling, and Applications*, John Wiley & Sons, Hoboken, New Jersey, USA.

Smith, B. and Arrillaga, J. (1999) 'Power flow constrained harmonic analysis in AC-DC power systems', *IEEE Transactions on Power Systems*, Vol. 14, No. 4, pp.1251–1261.

Thunberg, E. and Soder, L. (1999) 'A Norton approach to distribution network modeling for harmonic studies', *IEEE Transactions on Power Delivery*, Vol. 14, No. 1, pp.272–277.

Xia, D. and Heydt, G.T. (1982a) 'Harmonic power flow studies part I – formulation and solution', *IEEE Transactions on Power Apparatus and Systems*, Vol. PAS-101. No.6, pp.1257-1265.

Xia, D. and Heydt, G.T. (1982b) 'Harmonic power flow studies – part II implementation and practical application', *IEEE Transactions on Power Apparatus and Systems*, Vol. PAS-101, No. 6, pp.1266–1270.

Appendix

Table A1 Harmonic spectrum data at nonlinear buses (NLD)

Harmonic order	*NLD 1 at bus 12*		*NLD 2 at bus 32*		*NLD 3 at bus 33*		*NLD 4 at bus 66*		*NLD 5 at bus 67*	
	Mag (%)	*Ph (°)*	*Mag (%)*	*Ph (°)*	*Mag (%)*	*Ph (°)*	*Mag (%)*	*Ph (°)*	*Mag (%)*	*Ph (°)*
1	100	0	100	0	100	0	100	0	100	0
5	18.24	–55.68	4.24	–95.68	20	0	23.52	111	82.8	–135
7	11.9	–84.11	17.9	–74.11	14.3	0	6.08	109	77.5	69
11	5.73	–143.56	8.3	–113.56	9.1	0	4.57	–158	46.3	–62
13	4.01	–175.5	7.01	–194.58	7.7	0	4.2	–178	41.2	139
17	1.93	111.39	1.93	11.39	5.9	0	1.8	–94	14.2	9
19	1.39	68.3	2.39	38.3	5.3	0	1.37	–92	9.7	–155
23	0.94	–24.61	0.64	–4.61	4.3	0	0.75	–70	1.5	–158
25	0.86	–67.64	0.46	–17.64	4	0	0.56	–70	2.5	98

Table A2 Nonlinear load used in Algerian power system 114 bus

Nonlinear load		*POWER*	
Bus	*Name*	*MW*	*MVAR*
12	NLD1	1.2	0.75
32	NLD2	0.75	0.5
33	NLD3	1.3	0.6
66	NLD4	3	1.1
67	NLD5	1.8	0.7

Table A3 TCSC design parameters

TCSC location	*Inductance reactance X_L (p.u)*	*Capacitance reactance X_C (p.u)*	*Compensation level (%)*
TCSC (49-41)	0.0939	0.2112	50%